RiESTech
Recent in Engineering Science and Technology

MBI

Article

Failure Analysis of Economizer Tube Leakage Caused by Localized Internal Corrosion at Weld-Root Regions

Dede Rizka Ramadhan [1,*], Yudha Pratesa [1], Johny Wahyuadi Mudaryoto [1]

[1] Department of Metallurgical and Materials Engineering, Faculty of Engineering, Universitas Indonesia, Depok 16424, Indonesia
* Correspondence: dede.rizka@ui.ac.id

Abstract: Economizer tube leakage is a common failure in industrial boiler systems that can result in unplanned shutdowns and significant production losses. This study investigates the leakage failure of ASTM A210 Grade C economizer tubes removed from a pulp and paper boiler after long-term service. The investigation combined field inspection, wall-thickness measurements, chemical composition analysis, hardness testing, metallographic examination, and SEM–EDS characterization to determine the failure mechanism. Leakage was identified in Tube Row 99 and Tube Row 185 adjacent to circumferential and stopper-weld regions, where severe wall thinning was concentrated near the weld root while neighbouring tube sections remained largely unaffected. The minimum remaining wall thickness decreased from 3.00 mm to 1.85 mm. Chemical composition analysis confirmed compliance with ASTM A210 Grade C requirements, and hardness testing showed no evidence of abnormal hardening or thermal degradation, indicating that material nonconformity was not responsible for the failure. Metallographic examination revealed disruption of the protective oxide layer and corrosion penetration originating from the internal surface, while SEM–EDS analysis identified corrosion products dominated by iron oxides, confirming an internally initiated corrosion process. The morphology of the perforated regions demonstrated that corrosion propagated from the internal diameter toward the external surface, resulting in progressive wall thinning and through-wall perforation. Operating records indicated fluctuations in dissolved oxygen concentration that may have reduced oxide-layer stability and contributed to corrosion propagation. The failure mechanism was identified as weld-root-associated localized internal corrosion promoted by weld-root geometric irregularities, with dissolved oxygen fluctuations acting as a contributing rather than primary factor. These findings provide practical guidance for improving weld quality control, inspection planning, predictive maintenance, and boiler water chemistry management to reduce the risk of similar failures.

Keywords: Economizer tube; Failure analysis; Localized internal corrosion; Weld-root; SEM–EDS

Citation: Ramadhan, D. R., Pratesa, Y., Mudaryoto, J. W. (2026). Failure Analysis of Economizer Tube Leakage Caused by Localized Internal Corrosion at Weld-Root Regions. Recent in Engineering Science and Technology, 4(3), 139–154. Retrieved from https://www.mbi- journals.com/index.php/riestech/article/view/163.

Academic Editor: Yudhi Ariadi

Received: 6 June 2026
Accepted: 28 July 2026
Published: 31 July 2026

1. Introduction

Economizers are widely used in industrial boiler systems to improve thermal efficiency by recovering heat from flue gases and transferring it to feedwater before entering the steam drum (Subramanian, 2020; Incropera et al., 2021). During long-term operation, economizer tubes are continuously exposed to high-temperature water–steam environments that may promote corrosion, degradation of the protective oxide layer, and progressive wall thinning. These degradation processes can compromise tube integrity and eventually lead to leakage, resulting in unplanned shutdowns, production losses, and increased maintenance costs (Dooley, 2020; Gabrielli et al., 2021). ASTM A210 Grade C is a seamless medium-carbon steel extensively used for economizer and boiler tubes because of its good mechanical strength, weldability, and resistance to high-temperature water–steam service. Nevertheless, prolonged exposure to aggressive operating environments may still result in localized corrosion and progressive wall-thickness reduction, making this material an appropriate subject for failure analysis.

Leakage of economizer tubes has been associated with several degradation mechanisms, including internal corrosion, pitting attack, flow-accelerated corrosion, erosion-corrosion, and breakdown of protective oxide layers under unfavorable water chemistry conditions (Pal et al., 2020; Kumar et al., 2020; Duarte et al., 2021). In welded components, susceptibility to localized degradation may increase due to geometric discontinuities, residual stresses, and microstructural heterogeneity introduced during fabrication. These factors create localized electrochemical conditions that accelerate metal loss in specific regions of the tube (Kim et al., 2021; Ghosh et al., 2022).

Among welded regions, the weld-root area is particularly vulnerable because it is directly exposed to the internal water–steam environment. Excessive weld-root penetration or irregular root profiles may create crevice-like geometries that promote deposit accumulation, disturb local flow characteristics, and generate localized chemical environments favorable for corrosion initiation. Once the protective magnetite layer becomes unstable, corrosion preferentially develops beneath retained deposits at the weld-root region, resulting in localized wall thinning. Continued material loss eventually leads to through-wall perforation and tube leakage. Fluctuations in dissolved oxygen concentration may further reduce magnetite-layer stability, thereby increasing the susceptibility of weld-root regions to localized corrosion (Dooley, 2020; Li et al., 2022). These effects become more pronounced in geometrically restricted regions where stagnant flow conditions and oxygen concentration gradients may develop.

Failure of economizer tubes is particularly critical in continuous-process industries because even a single tube leakage may require boiler shutdown, resulting in substantial production losses and costly maintenance interventions. Numerous studies have investigated economizer tube failures associated with general internal corrosion, flow-accelerated corrosion, overheating, and fireside corrosion. However, direct metallurgical evidence linking weld-root geometric irregularities, oxide-layer deterioration, and localized internal corrosion remains limited. In particular, the role of weld-root morphology as a preferential corrosion-initiation site has not been thoroughly clarified using an integrated failure-analysis approach combining field observations, metallography, and SEM–EDS characterization. Consequently, the degradation sequence connecting weld-root geometry, localized corrosion development, wall-thickness reduction, and through-wall perforation remains insufficiently documented.

Therefore, this study investigates the leakage failure of ASTM A210 Grade C economizer tubes removed from a pulp and paper boiler after long-term service. The investigation integrates field inspection, wall-thickness measurements, chemical composition analysis, hardness testing, metallographic examination, and SEM–EDS characterization to establish the degradation sequence and identify the dominant failure mechanism responsible for leakage.

The novelty of this study lies in providing direct metallurgical evidence that weld-root geometric irregularities act as preferential sites for localized internal corrosion by promoting deposit retention and oxide-layer deterioration. By integrating field inspection, wall-thickness measurements, metallographic examination, and SEM–EDS characterization, this study reconstructs the degradation sequence from corrosion initiation to through-wall perforation and clarifies the interaction between weld-root geometry, oxide-layer instability, and localized corrosion under boiler operating conditions. The findings provide practical guidance for improving weld quality control, inspection planning, predictive maintenance, and boiler water chemistry management to reduce the risk of economizer tube failures in industrial boiler systems.

2. Materials and Methods

2.1. Sample Description

The investigated specimens were obtained from failed economizer tubes removed from a water-tube boiler operating in a pulp and paper facility following a scheduled boiler shutdown. Leakage was detected in the economizer section during routine operation, and two representative tubes exhibiting visible perforation adjacent to circumferential and stopper-weld joints were selected for detailed examination. The tubes were manufactured from ASTM A210 Grade C carbon steel and had been exposed to high-temperature water–steam service conditions for an extended operating period.

Visual inspection was performed as the initial stage of the failure investigation prior to specimen removal. Loose corrosion products and surface contaminants were carefully removed to expose the damaged regions, after which the tubes were examined by direct visual observation and documented using digital photographs. The inspection aimed to identify the location of leakage, characterize the visible damage, and evaluate its relationship with the welded joints before detailed laboratory examinations were conducted.

The visual inspection procedure consisted of: (1) identifying the leakage location within the economizer assembly; (2) recording the tube row identification and weld configuration; (3) examining the external tube surface for evidence of wall thinning, deformation, overheating, or mechanical damage; (4) observing the distribution of oxide deposits and corrosion products around the damaged regions; (5) documenting the morphology of the perforated areas and their relationship to the weld-root region; and (6) photographing representative damage for subsequent metallurgical evaluation.

The inspection data included tube identification, leakage location, weld type, visible wall-thinning characteristics, oxide-deposit distribution, corrosion-product accumulation, perforation morphology, and any evidence of external damage, overheating, or deformation. The inspection results were subsequently used to determine representative sampling locations for wall-thickness measurements, chemical composition analysis, hardness testing, metallographic examination, and SEM–EDS characterization as part of the integrated failure investigation.

2.2 Failure Assessment Procedure

The failure investigation was conducted through an integrated approach comprising visual inspection, wall-thickness measurement, material characterization, metallographic examination, and corrosion-product analysis to identify the degradation mechanism responsible for economizer tube leakage. The complementary results obtained from these examinations were integrated to reconstruct the degradation sequence leading to tube perforation.

Visual and macroscopic examination was performed to identify leakage morphology, corrosion distribution, and the relationship between damaged regions and welded joints (Pal et al., 2020; Oliveira et al., 2023). The examination included direct visual observation, documentation using digital photographs, and recording of corrosion products, oxide deposits, perforation morphology, and weld characteristics.

Wall-thickness measurements were carried out using an ultrasonic thickness gauge (Gauge: Olympus 38DL Plus, Olympus Corporation, Japan) in accordance with ASTM E797. After cleaning the tube surface, thickness readings were obtained at representative locations around the leakage region and adjacent unaffected areas to determine the remaining wall thickness.

Chemical composition was analyzed using an Optical Emission Spectrometer (OES) (Bruker Q4 TASMAN, Bruker, Germany) following ASTM A751. The specimen surface was ground and cleaned prior to analysis, and the measured composition was compared with the ASTM A210 Grade C specification.

Hardness testing was performed using a Rockwell hardness tester (Future-Tech FR-3, Japan) in accordance with ASTM E18 on the HRB scale. Five indentations were made in each of the base metal, weld metal, and heat-affected zone (HAZ), and the average hardness was calculated.

Metallographic specimens were prepared according to ASTM E3 and etched with a 2% Nital solution in accordance with ASTM E407. The specimens were examined using an optical microscope (Olympus BX53, Olympus Corporation, Japan) to characterize the microstructural features and corrosion penetration.

Corrosion morphology and corrosion products were characterized using a Scanning Electron Microscope (SEM) ([Manufacturer, Model, Country]) equipped with an Energy Dispersive Spectroscopy (EDS) detector (JEOL JSM-6510LV with Oxford Instruments EDS, Japan). SEM observations were conducted under high-vacuum conditions at an accelerating voltage of 15 kV, and the elemental composition of corrosion products was determined in accordance with ASTM E1508 and the procedure described by Tavares et al. (2022).

The experimental methods and characterization techniques employed in this investigation are summarized in Table 1.

Table 1. Experimental Methods and Characterization Techniques

Examination	Standard / Reference	Objective
Visual and Macroscopic Examination	Pal et al. (2020); Oliveira et al. (2023)	Identify leakage morphology, corrosion distribution, and degradation characteristics
Wall Thickness Measurement	ASTM E797; API RP 571	Quantify wall thinning and material loss
Optical Emission Spectrometry (OES)	ASTM A751	Verify material conformity with ASTM A210 Grade C
Hardness Testing	ASTM E18	Evaluate hardness variation across the weld region
Metallographic Examination	ASTM E3; ASTM E407	Characterize microstructural features and corrosion penetration
SEM–EDS Analysis	ASTM E1508; Tavares et al. (2022)	Identify corrosion morphology and corrosion products
Failure Mechanism Evaluation	API RP 571; Wang et al. (2023)	Correlate metallurgical evidence with leakage development

The examination methods summarized in Table 1 were selected to provide complementary information regarding the condition of the failed economizer tubes. Visual inspection and wall-thickness measurements established the location and extent of material degradation, while chemical composition analysis and hardness testing verified material conformity and mechanical integrity. Metallographic examination and SEM–EDS characterization were subsequently employed to investigate microstructural changes and corrosion-product formation. The combined findings from these complementary techniques were integrated to reconstruct the degradation sequence and identify the dominant failure mechanism responsible for economizer tube leakage.

3. Results and Discussion

The results of the failure investigation are presented in a systematic sequence by integrating the findings obtained from field inspection, wall-thickness measurements, material characterization, metallographic examination, SEM–EDS analysis, and operating history. Rather than interpreting each examination independently, the results from these complementary techniques are correlated to establish the origin of damage, evaluate the progression of material degradation, and identify the dominant failure mechanism responsible for economizer tube leakage.

3.1. Field Inspection and Macroscopic Examination

Field inspection was conducted during a scheduled boiler shutdown following the detection of leakage within the economizer section. The inspection focused on identifying leakage locations, corrosion distribution, damage morphology, and the condition of welded joints associated with the failed tubes. Leakage was identified in Tube Row 99 and Tube Row 185, both located near welded connections within the economizer assembly, as shown in Figure 2(a).

Visual examination revealed that the damage was confined to limited regions adjacent to the circumferential weld and stopper-weld interfaces rather than being uniformly distributed along the tube surface. The external surfaces of the affected tubes remained relatively intact and showed no indication of severe overheating, creep deformation, fireside corrosion, or mechanical damage. In contrast, oxide deposits and corrosion products were concentrated around the leakage locations, particularly on surfaces exposed to the internal water–steam environment.

The morphology of the perforated regions provides evidence regarding the progression of corrosion attack. In both failed tubes, the cavity opening was noticeably larger on the internal diameter (ID) side than on the external diameter (OD) side, indicating that material loss originated from the tube interior and advanced progressively through the wall thickness. Such morphology is characteristic of internally initiated corrosion and is inconsistent with damage arising from external exposure.

The failed tubes removed from service are presented in Figure 2(b), while close-up views of the perforated regions are shown in Figure 2(c). Leakage was concentrated near circumferential and stopper-weld locations where wall thinning and corrosion products were evident. In contrast, adjacent tube sections remained comparatively intact. The confinement of damage to the welded regions suggests that local geometric and environmental factors played a more significant role than generalized corrosion across the economizer tubing system. These observations were subsequently examined through thickness measurements and microstructural characterization to determine the mechanism responsible for leakage formation.

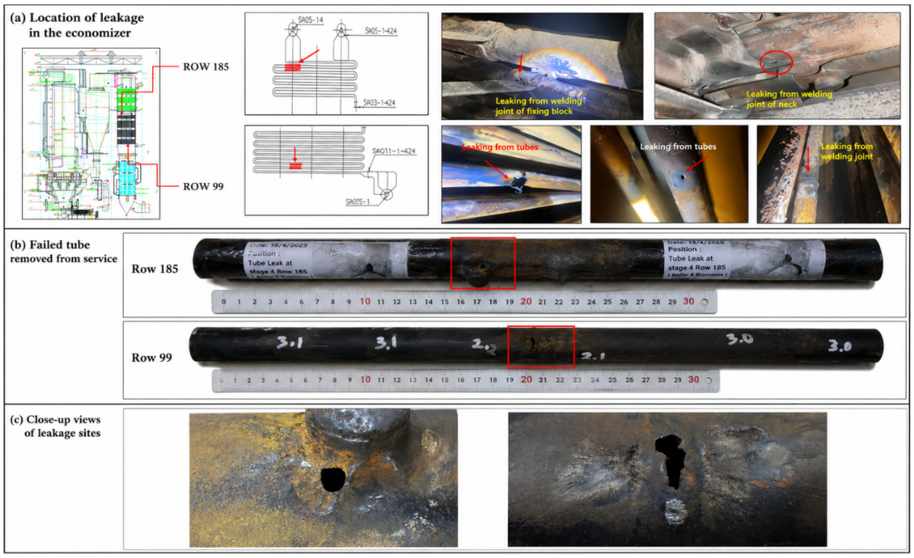

Figure 1. Field inspection and macroscopic appearance of failed economizer tubes.
(a) Leakage locations identified in Rows 99 and 185 during boiler shutdown inspection.
(b) Failed tubes removed from service showing the position of leakage.

(c) Close-up views of perforated regions adjacent to welded joints. The damage was concentrated near the weld-root vicinity, whereas adjacent tube surfaces remained comparatively unaffected.

Table 2. Summary of Field Inspection Findings

Location	Observation	Interpretation
Row 99	Leakage near circumferential weld	Localized internal corrosion
Row 185	Leakage near stopper weld	Weld-root-associated deterioration
Internal surface	Oxide deposits and corrosion products	Internally initiated degradation
Leakage morphology	Larger opening on ID side	ID-to-OD corrosion propagation

The field observations indicate that leakage originated from localized regions adjacent to the welded joints and progressed from the internal tube surface. However, visual inspection alone cannot determine whether the observed deterioration resulted from localized corrosion, material nonconformity, or changes in mechanical properties. Therefore, wall-thickness measurements, chemical composition analysis, and hardness testing were subsequently performed to quantify material loss, verify material conformity, and evaluate the integrity of the affected regions.

3.2. Material Characterization

Material characterization was conducted to evaluate the extent of wall thinning, verify material conformity, and assess whether changes in mechanical properties contributed to leakage formation.

Wall-thickness measurements revealed localized wall thinning in the vicinity of the leakage locations. The most severe reduction was identified in Tube Row 99, where the remaining wall thickness decreased from the nominal value of 3.00 mm to 1.85 mm. A similar pattern was observed in Tube Row 185, while adjacent regions retained considerably greater wall thickness. The uneven distribution of thickness loss indicates that material loss was concentrated near the welded regions rather than occurring uniformly across the tube surface. Representative wall-thinning features are shown in Figure 2, while the measurement results are summarized in Table 3.

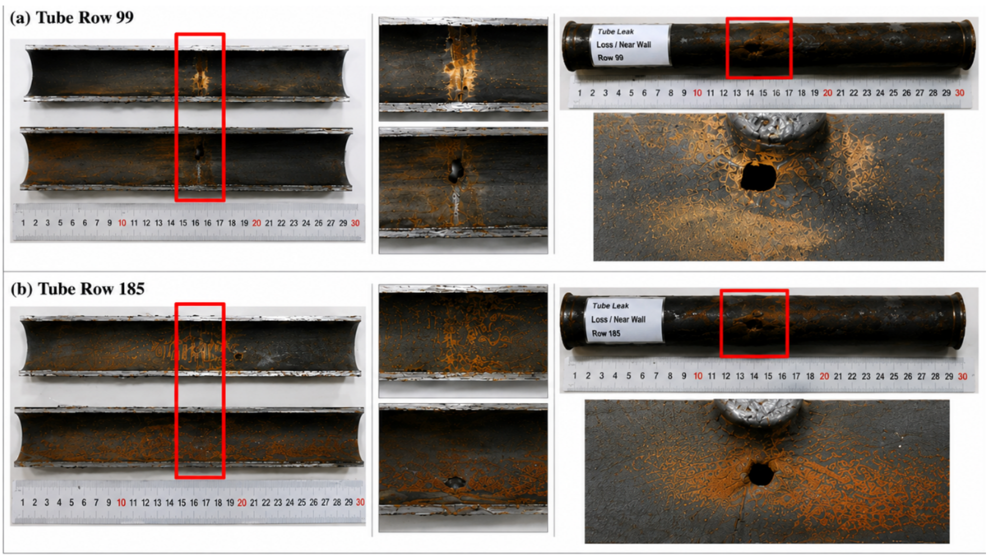

Figure 2. Wall thinning and perforation near welded regions.

(a) Tube Row 99 showing localized wall thinning and through-wall perforation adjacent to the welded region.
(b) Tube Row 185 exhibiting similar localized material loss and perforation near the weld penetration area. Damage was concentrated within confined regions, whereas surrounding tube sections remained comparatively unaffected.

Table 3. Thickness Measurement Results

No.	Tube Location / Row	Original Thickness (mm)	Remaining Thickness (mm)	Thickness Loss (mm)
1	Row 99 – Weld Region	3.00	1.85	1.15
2	Row 185 – Stopper Weld	3.00	2.10	0.90
3	Adjacent Non-Degraded Area	3.00	2.85	0.15

The thickness measurements confirm that material loss was highly localized and concentrated near the leakage locations. The substantial difference between the failed regions and adjacent tube sections indicates that deterioration progressed within confined areas rather than through uniform wall reduction across the tube surface.

Chemical composition analysis confirmed that the investigated tubes satisfied the requirements of ASTM A210 Grade C. The measured concentrations of carbon, manganese, silicon, phosphorus, sulfur, and other alloying elements remained within the specified limits. These findings indicate that material nonconformity was not associated with the observed leakage. The chemical composition results are presented in Table 4.

Table 4. Chemical Composition Results

Sample Code	C	Si	Mn	P	S	Fe
Good Tube	0.136	0.206	0.961	0.024	0.020	Bal.
Tube Row 185	0.187	0.212	0.863	0.017	0.020	Bal.
ASTM A210 Grade C	Max 0.35	Min 0.10	0.29–1.06	Max 0.035	Max 0.035	Bal.

The chemical composition data demonstrate that all measured elements remained within the specified limits. Therefore, the leakage failure cannot be attributed to deviations in chemical composition or material specification.

Hardness testing revealed only minor differences between the failed and unaffected tube sections. The measured hardness values remained within the expected range for ASTM A210 Grade C carbon steel and showed no evidence of abnormal hardening, embrittlement, or thermal degradation. These results indicate that significant changes in mechanical properties were unlikely to have contributed to leakage formation. The hardness results are summarized in Table 5.

Table 5. Hardness Test Results

Code	Indentation 1	Indentation 2	Indentation 3	Indentation 4	Indentation 5	Average Hardness (HRB)
Good Tube	84	86	86	85	85	85
Tube Row 185	89	90	89	90	91	90
ASTM A210 Grade C	-	-	-	-	-	Max 89

The hardness values obtained from the failed and unaffected specimens were generally comparable, with average hardness values of 90 HRB and 85 HRB, respectively. The hardness values obtained from the failed and unaffected specimens were generally comparable, with average hardness values of 90 HRB and 85 HRB, respectively. Although the average hardness of Tube Row 185 was marginally higher than that of the reference tube, the difference was small and remained within the expected variation for service-exposed ASTM A210 Grade C tubing. No localized hardness increase indicative of abnormal hardening, embrittlement, phase transformation, or thermal degradation was identified. Therefore, the hardness results suggest that changes in mechanical properties did not play a significant role in the leakage failure, the difference is considered insignificant and may be attributed to normal measurement variability associated with Rockwell hardness testing. No localized hardness increase indicative of abnormal hardening, embrittlement, phase transformation, or thermal degradation was identified. Therefore, the hardness results suggest that changes in mechanical properties did not play a significant role in the leakage failure. Collectively, the material characterization results indicate that neither material nonconformity nor mechanical-property variation was responsible for leakage formation. In contrast, localized wall thinning was consistently concentrated near the failed regions, highlighting progressive material loss as the most significant feature identified during this stage of the investigation. These findings suggest that the observed leakage was primarily associated with a localized corrosion process rather than metallurgical degradation. To determine the underlying cause of this localized deterioration, detailed metallographic and SEM–EDS examinations were subsequently performed.

3.3. Metallographic and SEM–EDS Analysis

Metallographic and SEM–EDS examinations were performed to investigate the damaged sections of the economizer tubes and identify the features associated with leakage development. The analysis focused on the area surrounding the weld root, where field inspection and thickness measurements revealed the greatest loss of material.

Cross-sectional observations revealed a marked contrast between the reference and failed specimens. The reference weld exhibited a sound profile and a continuous internal surface without visible signs of deterioration. In the failed specimen, a through-wall opening was present adjacent to the weld root. As illustrated in Figure 4(a–b), the perforation was wider on the internal diameter (ID) side than on the external diameter (OD) side, indicating that metal loss progressed outward from the tube interior. The geometry of the damaged area is characteristic of corrosion-driven wall reduction rather than mechanical rupture.

Representative microstructures from the base metal (BM), heat-affected zone (HAZ), and weld metal (WM) are shown in Figure 4(c–e). All examined regions displayed ferrite–pearlite structures typical of ASTM A210 Grade C carbon steel. No evidence of overheating, creep damage, abnormal phase transformation, or grain-boundary deterioration was observed. The microstructural features therefore remained consistent with those expected for the material under normal service conditions.

A different condition was observed at the damaged weld-root interface, shown in Figure 4(f). The affected area exhibited disruption of the oxide layer accompanied by corrosion penetration and significant wall reduction. Material removal was confined to a narrow zone adjacent to the weld root, whereas the surrounding microstructure remained largely intact. This observation agrees with the thickness measurements presented in Section 3.2 and confirms that degradation was concentrated within a restricted area of the tube wall.

Further evidence was obtained from SEM examination. The corroded surfaces were characterized by irregular topography, shallow cavities, and discontinuities within the oxide layer. These features became increasingly pronounced closer to the perforated region, reflecting progressive deterioration of the protective surface film during service exposure. Representative SEM images and EDS results are presented in Figure 5.

The EDS spectra and elemental maps revealed that the corrosion deposits were composed primarily of iron and oxygen, confirming the presence of iron-oxide products. Sulfur-rich compounds were not detected in significant quantities. This compositional evidence is consistent with degradation occurring under the internal water–steam environment and does not support external fireside corrosion as the governing process.

Taken together, the metallographic and SEM–EDS findings establish a consistent sequence of damage development. Breakdown of the protective oxide layer was followed by corrosion penetration and progressive wall reduction within the same confined location. As the remaining wall thickness decreased, a through-wall opening eventually formed, providing a direct path for leakage.

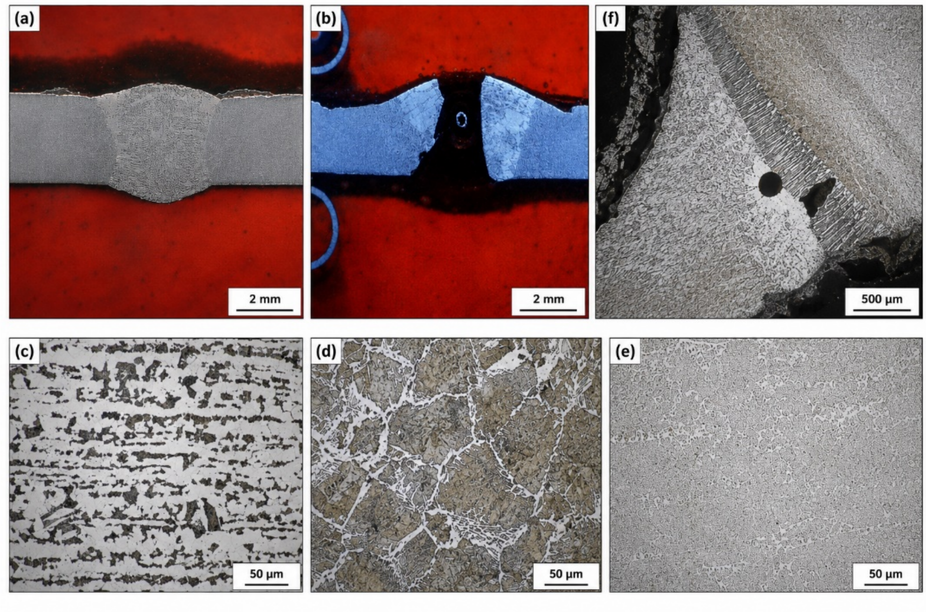

Figure 3. Metallographic comparison between reference and failed specimens.

(a) Reference weld cross section from a non-leaked tube.
(b) Failed weld cross section showing perforation adjacent to the weld-root interface.
(c) Base metal (BM).
(d) Heat-affected zone (HAZ).
(e) Weld metal (WM).
(f) Corrosion penetration and wall-thickness reduction at the weld-root interface.

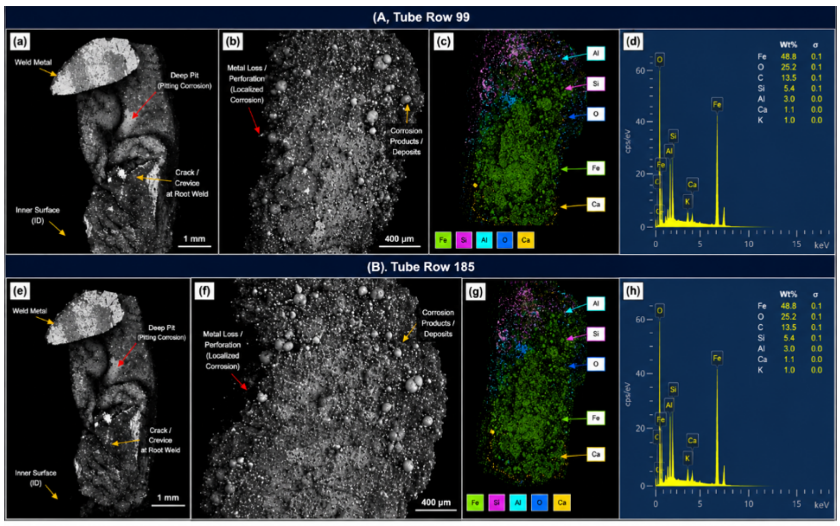

Figure 4. SEM–EDS characterization of leakage regions.

(A) Tube Row 99:
(a) SEM overview of the weld-root region,
(b) higher-magnification image of the perforated area,
(c) EDS elemental map of corrosion products, and
(d) corresponding EDS spectrum.

(B) Tube Row 185:
(e) SEM overview of the weld-root region,
(f) higher-magnification image of the perforated area,
(g) EDS elemental map of corrosion products, and
(h) corresponding EDS spectrum.

Table 6. Summary of Metallographic and SEM–EDS Observations

Observation	Interpretation
Ferrite–pearlite microstructure in BM, HAZ, and WM	Material characteristics remained consistent with ASTM A210 Grade C
No evidence of overheating, creep damage, or abnormal phase transformation	Thermal degradation did not contribute significantly to failure
Severe wall reduction adjacent to weld root	Material loss occurred within a confined region
Oxide-layer disruption near damaged areas	Breakdown of surface protection facilitated corrosion development
Corrosion penetration extending from ID toward OD	Damage originated from the internal surface
Iron-oxide corrosion products	Degradation occurred under water–steam service conditions
No significant sulfur enrichment	Fireside corrosion was not the governing mechanism

The metallographic and SEM–EDS findings are consistent with the field observations and wall-thickness measurements presented in the previous sections. The regions exhibiting the greatest wall reduction corresponded to localized oxide-layer deterioration and corrosion penetration adjacent to the weld root. Furthermore, SEM–EDS analysis confirmed that the corrosion products consisted predominantly of iron oxides, providing complementary evidence that the observed material loss resulted from an internally initiated corrosion process rather than external degradation or metallurgical instability.

3.4 Operating History and Water Chemistry

Although the available dissolved oxygen (DO) records were incomplete, the observed fluctuations, together with the metallographic and SEM–EDS findings, suggest that unstable oxygen conditions may have contributed to the corrosion process.

Figure 5. Record of Dissolved Oxygen (DO) at PB1

DO monitoring records from August to October 2025 are presented in Figure 5. The available measurements indicate dissolved oxygen (DO) concentrations ranging from approximately 1 to 19 ppb during the monitoring period. However, the records contain two intervals where no monitoring data were available, limiting the continuity of the dataset. Consequently, the available data are insufficient to establish a direct relationship between dissolved oxygen concentration and the observed corrosion behavior.

Although fluctuations in DO were observed in the available records, their influence on tube degradation cannot be conclusively determined because of the incomplete monitoring history. Nevertheless, the observed DO variations are consistent with the metallographic evidence of oxide-layer deterioration and the SEM–EDS identification of iron-oxide corrosion products. Therefore, dissolved oxygen fluctuations are interpreted as a possible contributing factor that may have influenced oxide-film stability, rather than as definitive evidence of the primary cause of economizer tube failure.

Fluctuations in dissolved oxygen are known to affect the stability of the protective magnetite layer on carbon-steel surfaces, thereby increasing susceptibility to localized corrosion. This effect may become more significant in geometrically restricted weld-root regions, where deposit accumulation and localized chemical variations can develop. Metallographic and SEM–EDS examinations revealed oxide-layer disruption, corrosion penetration, and localized wall thinning adjacent to the weld-root interface, supporting the role of oxygen instability as a contributing factor in the degradation process.

The values presented in Table 7 are generalized ranges compiled from industrial boiler chemistry guidelines and should be regarded as indicative rather than absolute corrosion-rate values.

Table 7. Corrosion Rate vs DO in Economizer Tube (Carbon Steel)

DO Level	Typical Corrosion Rate	Notes
< 5 ppb	< 0.1 mpy	Protective magnetite layer stable
5–10 ppb	0.1–0.5 mpy	Generally acceptable for high-pressure systems
10–20 ppb	0.5–2 mpy	Increased tendency for pitting initiation
20–50 ppb	2–10 mpy	Localized deep pits commonly observed
50–200 ppb	10–50 mpy	Severe pitting associated with tube failures
> 200 ppb	> 50 mpy	Rapid tube penetration may occur

Table 7 illustrates the general relationship between dissolved oxygen concentration and corrosion behavior in carbon-steel economizer tubes. Low DO levels generally promote the stability of the protective magnetite layer, whereas elevated or fluctuating DO concentrations may increase the tendency for localized corrosion and pitting. Although the available operational records do not establish a direct quantitative correlation between DO and corrosion rate, the observed fluctuations are consistent with conditions that may accelerate oxide-layer deterioration and localized corrosion development near the weld-root region.

3.5 Failure Mechanism Discussion

The results obtained from field inspection, wall-thickness measurements, metallographic examination, and SEM–EDS characterization provide a consistent explanation for the leakage observed in the economizer tubes. The damage originated from the internal surface and developed progressively within a confined region adjacent to the weld root. Unlike generalized corrosion, deterioration was concentrated at specific locations while neighbouring tube sections remained comparatively unaffected.

Leakage was identified in Tube Row 99 and Tube Row 185 near circumferential and stopper-weld interfaces. Thickness measurements showed that the most severe wall reduction occurred in these regions, where the remaining thickness was significantly lower than the nominal tube wall. The confinement of material loss to areas adjacent to welded joints suggests that local conditions governed the degradation process rather than uniform corrosion throughout the economizer tubing system.

The weld-root geometry is considered a key factor influencing damage initiation. Geometric irregularities at the weld-root interface can alter local flow characteristics and promote the retention of deposits and corrosion products. The accumulation of these species may create localized chemical conditions that differ from those on the surrounding tube surface. Under such circumstances, the stability of the protective oxide layer can be reduced, increasing susceptibility to corrosion attack.

Metallographic examination revealed disruption of the oxide layer together with corrosion penetration in the damaged regions. In contrast, the base metal, heat-affected zone, and weld metal retained ferrite–pearlite microstructures characteristic of ASTM A210 Grade C carbon steel. No evidence of overheating, creep damage, grain-boundary deterioration, or abnormal phase transformation was observed. These findings indicate that the leakage event was not associated with thermal degradation or metallurgical instability.

The morphology of the perforated areas provides direct evidence of the direction of degradation. Cross-sectional observations showed that the cavity opening was larger on the internal diameter (ID) side than on the external diameter (OD) side. This feature indicates that corrosion progressed from the internal surface toward the outer wall. The same regions also exhibited the greatest wall reduction, establishing a direct relationship between corrosion penetration and material loss.

SEM observations identified corrosion cavities, irregular surface morphology, and discontinuities within the oxide layer surrounding the leakage locations. EDS analysis showed that the corrosion deposits consisted predominantly of iron and oxygen, confirming the presence of iron-oxide products formed during service exposure. Sulfur-bearing compounds were not detected in significant quantities, indicating that external fireside corrosion was not the governing degradation mechanism.

Operational records indicated fluctuations in dissolved oxygen (DO) concentration during boiler operation. Although oxide-film stability was not measured directly, variations in dissolved oxygen are known to influence the formation and persistence of protective magnetite layers on carbon-steel surfaces. In areas where geometric discontinuities and deposit accumulation already exist, disturbances in oxide stability may increase the likelihood of corrosion activity. The weld-root region therefore provided favourable conditions for continued degradation once the protective oxide layer had been compromised.

The collective findings indicate a degradation sequence in which oxide-layer deterioration was followed by corrosion penetration and progressive wall reduction near the weld root. As material loss continued, the remaining wall thickness gradually decreased until a through-wall perforation was formed. Leakage occurred when the tube wall could no longer maintain pressure containment under normal operating conditions.

The proposed degradation sequence is illustrated in Figure 6, while the relationship between the immediate cause of leakage and the underlying contributing factors is summarized in the Root Cause Failure Analysis (RCFA) presented in Figure 7. Both models are consistent with the field observations, thickness measurements, metallographic findings, and SEM–EDS results obtained throughout the investigation.

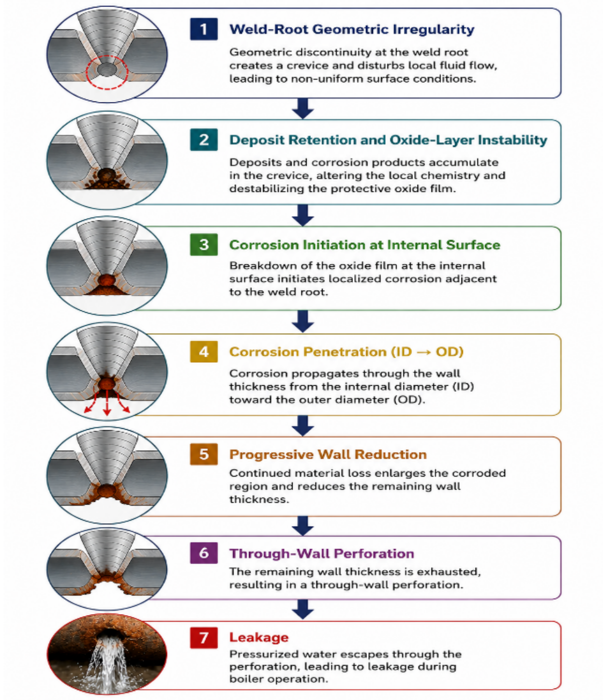

Figure 6. Sequential degradation mechanism of economizer tube failure associated with weld-root geometric irregularities.

Geometric irregularities at the weld-root interface promoted deposit retention and disturbed local flow conditions, creating a favorable environment for oxide-layer instability. The resulting breakdown of the protective oxide layer initiated localized corrosion at the internal tube surface. Corrosion subsequently propagated from the internal diameter (ID) toward the external diameter (OD), causing progressive wall thinning adjacent to the weld root. Continued material loss reduced the remaining wall thickness until through-wall perforation occurred, allowing pressurized water to escape and resulting in tube leakage during service operation.

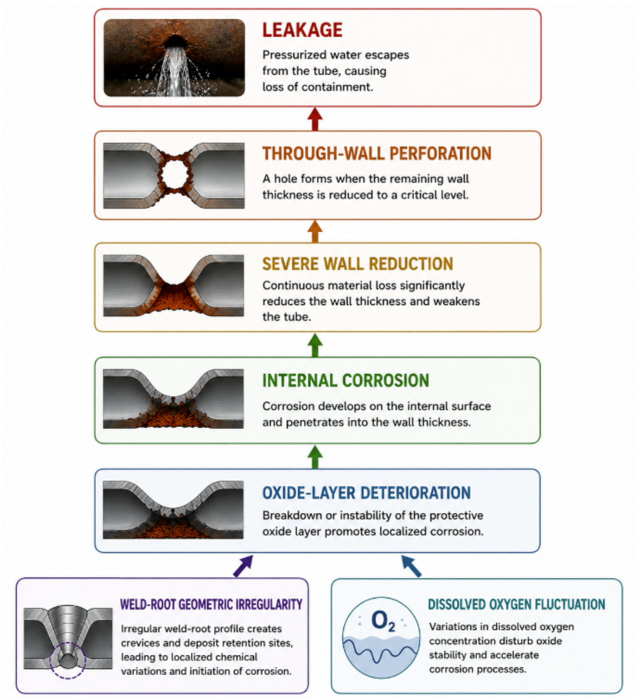

Figure 7. Root Cause Failure Analysis (RCFA) of economizer tube leakage.

Figure 7. Root Cause Failure Analysis (RCFA) of economizer tube leakage. Leakage resulted from through-wall perforation caused by severe wall reduction. The wall reduction developed through internal corrosion associated with oxide-layer deterioration. The underlying contributing factors were weld-root geometric irregularities and fluctuations in dissolved oxygen concentration, which promoted sustained corrosion activity near the internal tube surface.

4. Conclusions

A comprehensive failure investigation was conducted on ASTM A210 Grade C economizer tubes removed from service following leakage in a water-tube boiler operating at a pulp and paper facility. Representative findings indicate that leakage was consistently confined to the weld-root regions, where severe localized wall thinning, oxide-layer deterioration, and internally initiated corrosion were observed, while the material retained its specified chemical composition, microstructure, and mechanical properties. These representative findings demonstrate that the leakage resulted from localized degradation associated with internally initiated corrosion rather than material nonconformity or thermal degradation.

Based on the integrated findings, the following conclusions are drawn:

1. Leakage was localized in Tube Row 99 and Tube Row 185 adjacent to circumferential and stopper-weld interfaces. Severe wall thinning was concentrated near the weld-root regions, whereas adjacent tube sections remained comparatively unaffected, indicating a localized degradation process.
2. The tubes satisfied the requirements of ASTM A210 Grade C and exhibited no evidence of metallurgical instability, abnormal hardening, overheating, creep damage, or phase transformation. Therefore, material nonconformity and thermal degradation were excluded as the primary causes of failure.
3. Metallographic examination revealed oxide-layer deterioration and corrosion penetration originating from the internal tube surface, while SEM–EDS analysis confirmed corrosion products dominated by iron oxides. The absence of significant sulfur enrichment further indicates that fireside corrosion was not the governing degradation mechanism.
4. The morphology of the perforated regions demonstrated that corrosion propagated from the internal diameter toward the external surface, resulting in progressive wall thinning and eventual through-wall perforation.
5. The dominant failure mechanism was identified as weld-root-associated localized internal corrosion. Weld-root geometric irregularities promoted deposit accumulation that facilitated corrosion initiation, while fluctuations in dissolved oxygen are considered a contributing factor that may have reduced oxide-layer stability and facilitated corrosion propagation.

Overall, the investigation demonstrates that economizer tube leakage resulted from the combined effects of weld-root geometric irregularities, oxide-layer deterioration, and progressive internally initiated corrosion. Improving weld-root quality, implementing periodic inspection of susceptible welded regions, and maintaining effective boiler water chemistry control are recommended to reduce the risk of similar failures during long-term operation.

Acknowledgments: The authors gratefully acknowledge the operating company for providing access to operational records, field inspection activities, and failed economizer tube samples used in this investigation. Appreciation is also extended to the technical personnel for their assistance with specimen preparation, metallographic examination, and material characterization. Their support was essential to the successful completion of this study.

Author Contributions

Conceptualization, D.R.R. and Y.P.; Methodology, D.R.R. and Y.P.; Investigation, D.R.R.; Formal analysis, D.R.R.; Data curation, D.R.R.; Writing – original draft preparation, D.R.R.; Writing – review and editing, Y.P.; Supervision, Y.P. All authors have read and agreed to the published version of the manuscript.

Funding

This research received no external funding.

Conflicts of Interest

The authors declare no conflict of interest.

References

1. Subramanian P. Deterioration of economizer tubes in utility boilers. Engineering Failure Analysis. 2020;112:104515.
2. Dooley RB. Boiler tube failures associated with oxygen corrosion and magnetite instability. PowerPlant Chemistry. 2020;22(6):321–330.
3. Gabrielli F, et al. Water chemistry related tube failures in industrial boilers. Materials at High Temperatures. 2021;38(2):112–124.
4. Pal S, et al. Failure analysis of boiler economizer tubes at power house. Engineering Failure Analysis. 2020;97:1–10.
5. Kumar P, et al. Root cause failure analysis of industrial boiler tubes. Engineering Failure Analysis. 2020;118:104866.
6. Duarte CA, et al. Failure analysis of water-tube boiler components under corrosive environment. Engineering Failure Analysis. 2021;119:104983.
7. Ghosh S, et al. Localized corrosion behavior in welded boiler tubes under high-temperature service. Journal of Failure Analysis and Prevention. 2022;22:455–468.
8. Li H, et al. Failure assessment of carbon steel boiler tubes subjected to dissolved oxygen attack. Materials Today Communications. 2022;33:104598.
9. Oliveira P, et al. Failure investigation of economizer tube leakage by metallographic and SEM analysis. Engineering Failure Analysis. 2023;148:107183.
10. Wang L, et al. Corrosion failure in welded economizer tubes under high dissolved oxygen conditions. Engineering Failure Analysis. 2023;151:107412.
11. ASM International. Failure Analysis and Prevention. ASM Handbook. Vol. 11. Materials Park (OH): ASM International; 2020.
12. American Society of Mechanical Engineers. Boiler and Pressure Vessel Code, Section I: Power Boilers. New York: ASME; 2021.
13. ASTM International. ASTM A210/A210M: Standard Specification for Seamless Medium-Carbon Steel Boiler and Superheater Tubes. West Conshohocken (PA): ASTM International; 2021.
14. ASTM International. ASTM A751: Standard Test Methods, Practices, and Terminology for Chemical Analysis of Steel Products. West Conshohocken (PA): ASTM International; 2021.
15. ASTM International. ASTM E3: Standard Guide for Preparation of Metallographic Specimens. West Conshohocken (PA): ASTM International; 2021.
16. ASTM International. ASTM E18: Standard Test Methods for Rockwell Hardness of Metallic Materials. West Conshohocken (PA): ASTM International; 2021.
17. ASTM International. ASTM E407: Standard Practice for Microetching Metals and Alloys. West Conshohocken (PA): ASTM International; 2021.
18. ASTM International. ASTM E797/E797M: Standard Practice for Measuring Thickness by Manual Ultrasonic Pulse-Echo Contact Method. West Conshohocken (PA): ASTM International; 2021.
19. ASTM International. ASTM E1508: Standard Guide for Quantitative Analysis by Energy-Dispersive Spectroscopy. West Conshohocken (PA): ASTM International; 2021.

20. American Petroleum Institute. API Recommended Practice 571: Damage Mechanisms Affecting Fixed Equipment in the Refining Industry. Washington (DC): American Petroleum Institute; 2021.
21. American Petroleum Institute. API Standard 570: Piping Inspection Code: In-Service Inspection, Rating, Repair, and Alteration of Piping Systems. Washington (DC): American Petroleum Institute; 2024.
22. Baboian R. Corrosion Tests and Standards: Application and Interpretation. West Conshohocken (PA): ASTM International; 2020.
23. Callister WD Jr, Rethwisch DG. Materials Science and Engineering: An Introduction. 10th ed. Hoboken (NJ): Wiley; 2021.
24. Tavares S, et al. SEM–EDS evaluation of oxide deposits in boiler economizer tubes. Materials Characterization. 2022;193:112187.